AGU PUBLICATIONS

JGR

Journal of Geophysical Research: Solid Earth

RESEARCH ARTICLE
10.1002/2015JB011940

Key Points:
- Ionic impurities from sand have a doping effect on methane hydrate conductivity
- Methane hydrate provides the primary conduction path within mixtures with sand
- Results help model the effects of impurities on systems devoid of pore water

Supporting Information:
- Figure Data S1
- Sections S1 and S2, Table S1, and Figures S1–S3

Correspondence to:
W. L. Du Frane,
Wyatt.DuFrane@asu.edu

Citation:
Du Frane, W. L., L. A. Stern, S. Constable, K. A. Weitemeyer, M. M. Smith, and J. J. Roberts (2015), Electrical properties of methane hydrate + sediment mixtures, *J. Geophys. Res. Solid Earth*, *120*, 4773–4783, doi:10.1002/2015JB011940.

Received 10 FEB 2015
Accepted 23 JUN 2015
Accepted article online 25 JUN 2015
Published online 30 JUL 2015

Electrical properties of methane hydrate + sediment mixtures

Wyatt L. Du Frane[1], Laura A. Stern[2], Steven Constable[3], Karen A. Weitemeyer[3,4], Megan M. Smith[1], and Jeffery J. Roberts[1]

[1]Lawrence Livermore National Laboratory, Livermore, California, USA, [2]U. S. Geological Survey, Menlo Park, California, USA, [3]Scripps Institution of Oceanography, La Jolla, California, USA, [4]National Oceanography Centre Southampton, University of Southampton Waterfront Campus, Southampton, UK

Abstract Knowledge of the electrical properties of multicomponent systems with gas hydrate, sediments, and pore water is needed to help relate electromagnetic (EM) measurements to specific gas hydrate concentration and distribution patterns in nature. Toward this goal, we built a pressure cell capable of measuring in situ electrical properties of multicomponent systems such that the effects of individual components and mixing relations can be assessed. We first established the temperature-dependent electrical conductivity (σ) of pure, single-phase methane hydrate to be ~5 orders of magnitude lower than seawater, a substantial contrast that can help differentiate hydrate deposits from significantly more conductive water-saturated sediments in EM field surveys. Here we report σ measurements of two-component systems in which methane hydrate is mixed with variable amounts of quartz sand or glass beads. Sand by itself has low σ but is found to increase the overall σ of mixtures with well-connected methane hydrate. Alternatively, the overall σ decreases when sand concentrations are high enough to cause gas hydrate to be poorly connected, indicating that hydrate grains provide the primary conduction path. Our measurements suggest that impurities from sand induce chemical interactions and/or doping effects that result in higher electrical conductivity with lower temperature dependence. These results can be used in the modeling of massive or two-phase gas-hydrate-bearing systems devoid of conductive pore water. Further experiments that include a free water phase are the necessary next steps toward developing complex models relevant to most natural systems.

1. Introduction

Gas hydrates are clathrate structures of H_2O that encage gases of small molecular diameter, such as methane, ethane, propane, and CO_2 [*Sloan and Koh*, 2007]. The formation of gas hydrates typically requires moderately low temperatures, high pressure, and sufficient quantities of water and free- or dissolved-phase hydrate-forming gas. Such conditions occur globally—and often extensively—in permafrost regions and shallow marine environments such as in seafloor sediments along continental margins [*Kvenvolden and Lorenson*, 2001]. Consequently, gas hydrates are very common in these regions and harbor a significant hydrocarbon source that is of keen interest for economic as well as geohazard considerations [e.g., *Kvenvolden*, 1999; *Collett*, 2002; *Ruppel*, 2007; *Maslin et al.*, 2010; *Boswell and Collett*, 2011]. Estimates of the total global hydrate inventory have varied by up to 4 orders of magnitude [e.g., *Kvenvolden*, 1999; *Milkov*, 2004], with more recent estimates predicting that the amount of carbon bound by gas hydrates is greater than the total amounts in the atmosphere plus conventional natural gas reserves [*Boswell and Collett*, 2011; *Wallmann et al.*, 2012]. Estimates continue to improve with significant advances in global modeling and geophysical mapping of gas hydrate inventories [*Maslin et al.*, 2010; *Boswell and Collett*, 2011].

Traditional methods for geophysical detection of gas hydrates include well-logging and seismic surveys. Well-logging provides point measurements of gas hydrate concentration versus depth but is expensive and invasive. Seismic methods are also used to map the spatial distribution of gas hydrate deposits. The presence of a bottom simulating reflector may indicate the phase boundary between gas hydrate and free gas [e.g., *Hornbach et al.*, 2003]. This boundary alone, however, provides little information about the amount and distribution of gas hydrate above it. Seismic blanking zones can be used in some cases to help predict gas hydrate occurrence [e.g., *Hornbach et al.*, 2003; *Zhang and McMechan*, 2006]. Additional geophysical methods are clearly needed to obtain a more complete picture of gas hydrate distribution.

Electrical methods can be effective in remotely detecting gas hydrate due to the sensitivity of electrical properties to the compositions and microstructures of sedimentary materials [*Edwards*, 1997]. Gas hydrates have low electrical conductivity (σ—note that this is the inverse of resistivity: $\rho = \sigma^{-1}$) that provides a suitable target for marine controlled source electromagnetic (CSEM) surveys. CSEM sounding measures the amplitude and phase of electromagnetic (EM) energy propagating through the seafloor at one or more frequencies, and these data can be inverted to obtain the spatial distribution of conductivity. The combined use of both seismic and EM methods can help distinguish between gas (low velocity and high resistivity) and gas hydrate (high velocity and high resistivity) to map both the upper and lower boundaries of gas hydrate deposits. Pilot CSEM studies have demonstrated the sensitivity of this method in assessing general gas hydrate concentration, saturation, and distribution patterns [e.g., *Schwalenberg et al.*, 2005; *Evans*, 2007; *Weitemeyer et al.*, 2006, 2011]. Quantifying the estimates of hydrate volume, however, requires knowledge of the electrical conductivity of gas hydrates in combination with petrophysical mixing relations established from theory and experiment [*Collett and Ladd*, 2000; *Ellis et al.*, 2008].

Several previous laboratory studies focused on the electrical properties of gas hydrates in mixtures with sediment and water [*Spangenberg and Kulenkampff*, 2006; *Lee et al.*, 2010; *Ren et al.*, 2010]. The electrical conductivity of CH_4 hydrate was measured during formation from liquid water in the pore space of glass beads [*Spangenberg and Kulenkampff*, 2006] and quartz sand [*Ren et al.*, 2010]. A similar study examined electrical conductivity before and after gas hydrate formation within sandy sediments, using brine with 3.35 wt % NaCl [*Li et al.*, 2012]. These measurements are important for helping resolve mixing laws, but they are dominated by the presence of water, which obscures quantitative information on the more subtle contributions by gas hydrate or sediments to the overall electrical conductivity. Geometrical mixing laws, such as Archie's law or Hashin-Shtrikman lower bounds models, can be used with the assumption that gas hydrate has low σ compared to the surrounding seawater [*Archie*, 1942; *Hashin and Shtrikman*, 1962; *Glover et al.*, 2000]. This assumption is valid when the conductive pore water phase dominates the bulk conductivity—which is in fact the common mode in nature—but may not be valid where gas hydrate (the low conductivity phase) occurs in massive form or otherwise dominates bulk conductivity. The latter case can be especially important for mapping hydrate formations that are impermeable to gas, as they may also be relatively impermeable to pore water [e.g., *Kneafsey et al.*, 2011]. *Lee et al.* [2010] published a systematic examination of electrical conductivity and permittivity (electric field response) for water-free tetrahydrofuran (THF) hydrate mixed with sand, silts, and clay, but as THF hydrate is only an analog for natural gas hydrate, it may have different conduction mechanisms due to its different molecular structure as a structure II hydrate versus the more common naturally occurring structure I (sI) hydrate.

Lastly, the previous studies have not carefully examined the temperature dependence of the electrical conductivity gas hydrate/sediment mixtures. Most electrical insulators, such as gas hydrates, have electrical conductivity that increases exponentially with increasing temperature. Details of this relationship can yield important mechanistic information about conduction mechanisms [e.g., *Roberts*, 2002], which must be understood to properly apply laboratory measurements to the widely varying conditions that exist in the field.

Du Frane et al. [2011] published the first direct measurements of the electrical conductivity of single-phase CH_4 hydrate formed from reacting high purity H_2O and CH_4. The σ of CH_4 hydrate ranged between 10^{-5} and 10^{-4} S/m for temperatures between −15 and 15°C, indicating strong, positive temperature dependence. These results were obtained in a custom-built pressure cell designed to allow synthesis of increasingly complex gas hydrate + sediment ± water mixtures, in which electrical conductivity can be measured in situ during both formation and dissociation of the hydrate phase. This method allows for controlled and predetermined mixing and textural arrangement of the various components in the system, meaning that the effects of individual components can be assessed for better integration into mixing models. In this study, we present new electrical conductivity results for the two-component system of fully reacted (i.e., water-free) methane hydrate in mixtures with varying proportions of sediments (quartz sand and glass beads) for a range of temperatures between −15 and 15°C.

We note that many—if not most—gas hydrate systems in nature contain a pore water component that dominates the overall electrical properties of the system; hence, results from multicomponent samples that include a pore water phase will obviously be critical for modeling most systems in nature. However,

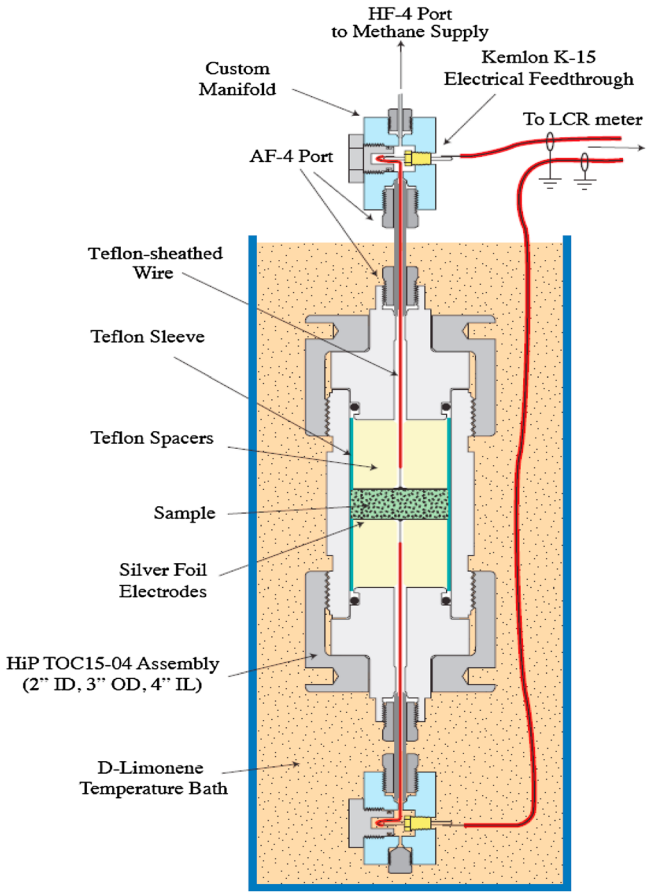

Figure 1. Pressure vessel designed to synthesize gas hydrate and measure impedance spectroscopy in situ [from *Du Frane et al.*, 2011].

massive gas hydrate formations that are lacking in pore water are expected to be present in some locations in nature, and such units could be of high economic value. Measuring electrical conductivity of mixed-phase systems in which there is no knowledge of the competing effects of the separate components, how the various components are positioned or connected within the system, or in what manner individual conduction mechanisms influence total conductivity, would simply yield isolated and ambiguous measurements due to the numerous unknowns. Also, the more subtle effects of adding sediment to gas hydrate would be eclipsed when adding an additional free water phase, and the only way to investigate such effects is by careful measurement of liquid-free systems. Future experiments are anticipated to incorporate a free water phase into the system in order to help develop the more complex models relevant to most natural systems.

2. Experimental Techniques

We developed a cell to synthesize gas hydrate and simultaneously measure electrical conductivity (Figure 1). The apparatus is built around a commercially available pressure vessel (High Pressure Equipment Company) with the addition of high-pressure manifolds on each end cap. Each manifold has a single port feed-through where methane gas and electrical leads enter into the vessel. Samples were 2.0″ in diameter and 0.5″ thick and were sandwiched by silver electrodes and Teflon spacers. Methane hydrate was synthesized in the pressure cell using a temperature cycling technique that enables full reaction of H_2O ice "seeds" and pressurized CH_4 (15–30 MPa) to polycrystalline CH_4 hydrate in a reproducible manner [*Stern et al.*, 1996, 2004]. The reactant ice seeds were made from a block of nearly gas-free ice that was grown from distilled-deionized water, then crushed and sieved to 0.180–0.250 mm.

Starting samples were prepared from granular ice that was free of sediment, mixed with quartz sand, or mixed with silica glass beads. The quartz sand and glass beads were not washed prior to use. Mixtures were made in proportions ranging from pure (100%) ice down to 10 vol % ice and 0–90 vol % sand or beads, with percentages referring to the solid phase only. All samples initially contained ~30–40% porosity, determined from mass measurements of each phase prior to mixing and packing into the known-volume sample chamber. Ice-only samples had highest initial porosity given their relatively uniform grain size compared to mixed-phase samples. In all samples, porosity reduces during reaction due to the ~16% volumetric increase of the H_2O phase that accompanies the ice to hydrate reaction, assuming density of ice and an empty sI hydrate lattice to be 917 and 790 kg/m^3, respectively [*Dvorkin et al.*, 2000]. Porosity of final samples is thus easily calculated, and the issue of porosity has been discussed previously in *Du Frane et al.* [2011]. For mixtures with sand, we used Oklahoma #1 (OK #1) high-purity quartz (SiO_2) sand that had minor hematite, illite, calcite, and alumina ($<$1 vol % combined) and a narrow grain size distribution with 84% of grain diameters between 0.106 to 0.250 mm [*Durham et al.*, 2009]. Two sample mixtures contained glass beads (Cataphote) made of high-purity soda-lime-silica (amorphous SiO_2 with a

Table 1. Summary of Sample Compositions, Run Conditions, and Equation (1) Fits for Parameters σ_0 and E_a

Sample	H_2O Phase	H_2O (vol %[a])	SiO_2 (vol %[a])	*T* cycles	P (MPa)	Dissociation *T* (°C)	Dissociation *t* (days)	Log (σ_0 (S/m))	E_a (kJ/mol)
					Run without sediment				
Run 1[b]	synthetic test	100.0	0.0	n/a	16.9–25.8	not applicable (n/a)	n/a	n/a	n/a
Run 2[b]	hydrate	100.0	0.0	10	18.3–21.3	−15	1	0.965	27.9
	ice	100.0	0.0		0.0			6.63	54.5
Run 3[b]	hydrate	100.0	0.0	7	16.2–18.5	−15	13	1.50	30.6
	ice	100.0	0.0		0.0			5.00	45.5
					Runs with OK#1 quartz sand				
Run 5	hydrate	90.0	10.0	8	23.8–26.4	−15	8	1.78	31.3
	ice	88.7	11.3		0.0			5.71	50.7
Run 6	hydrate	70.0	30.0	13	18.2–23.3	−3	11	2.42	33.7
	ice	67.0	33.0		0.0			6.49	50.7
Run 4	hydrate	57.7	42.3	16	21.5–25.7	n/a	n/a	−2.02	7.66
	ice	54.2	45.8		n/a			n/a	n/a
Run 8	hydrate	57.7	42.3	12	20.0–23.4	−3	6	−2.13	6.52
	ice	54.2	45.8		0.0			4.92	41.5
Run 10	hydrate	10.0	90.0	13	20.2–24.3	−3	6	−4.90	−0.503
	ice	8.8	91.2		0.0			−4.24	2.07
					Runs with soda-lime-silica beads				
Run 7	hydrate	57.2	42.8	15	6.1–9.1	−3	9	n/a	n/a
	ice	53.8	46.2		0.0			n/a	n/a
Run 9	hydrate	57.7	42.3	7	18.8–22.7	n/a	n/a	0.227	23.4
	ice	54.3	45.7		n/a			n/a	n/a

[a]Excludes porosity.
[b]Data from *Du Frane et al.* [2011].

small amount of Na_2CO_3 [*NIIR Board of Consultants and Engineers*, 2005]) glass with diameters ranging between 0.105 and 0.125 mm. Sample mixtures and run conditions are listed in Table 1.

The cell was first loaded with seed ice ± sediments and placed under methane pressure in a temperature controlled bath of inert coolant, d-Limonene. Heating the reactants above the ice point to conditions well within the methane hydrate stability field promoted full and efficient reaction to hydrate. The first run was carried out with one manifold replaced by a thermocouple to calibrate and monitor the synthesis reaction; any unreacted H_2O remaining after the heating stage was easily discernible by a discontinuity in the pressure-temperature curve upon cooling the sample below the ice point, in which case additional heating cycles were implemented. Subsequent runs were then performed without a thermocouple in the sample, using the σ measurement itself as an indicator of complete reaction, as it was similarly sensitive to excess liquid when cycling past the freezing/melting point. Samples were cycled multiple (≥7) times to ensure full reaction. During experiments, temperature and electrical conductivity were monitored and recorded throughout formation, stabilization, and dissociation.

Impedance spectroscopy data (20 Hz to 2 MHz) were collected with an Agilent E4980A LCR (inductance, capacitance, and resistance) meter throughout each run. The spectra were used to determine what frequency impedance measurement is needed to calculate the true electrical conductivity of the sample while excluding systemic contributions [e.g., *Roberts and Tyburczy*, 1991, 1993]. It should be noted that the range of frequencies swept during impedance spectroscopy measurements in the laboratory is unrelated to the frequencies used in CSEM field measurements. Our previous equivalent circuit modeling [*Du Frane et al.*, 2011] indicates that conductivity can be measured reliably at the frequency associated with the smallest capacitance to isolate the electrical response of our samples and avoid systemic effects, such as electrode polarization at low frequency. Measurements were performed on samples with fully reacted CH_4 hydrate between −15 and 15°C after seven or more automated temperature cycles. Heating was isochoric such that the pore pressure of CH_4 gas increased during the measurement (pressure ranges are listed in Table 1). Comparative impedance measurements were also performed between −15 and −2°C on several samples after the CH_4 hydrate was dissociated back into ice by venting CH_4 from the vessel at temperatures ≤−3°C for ≥6 days (Table 1). Single-frequency electrical conductivity (typically at 100 kHz) was monitored during CH_4 hydrate synthesis and dissociation to verify completion of each reaction. We

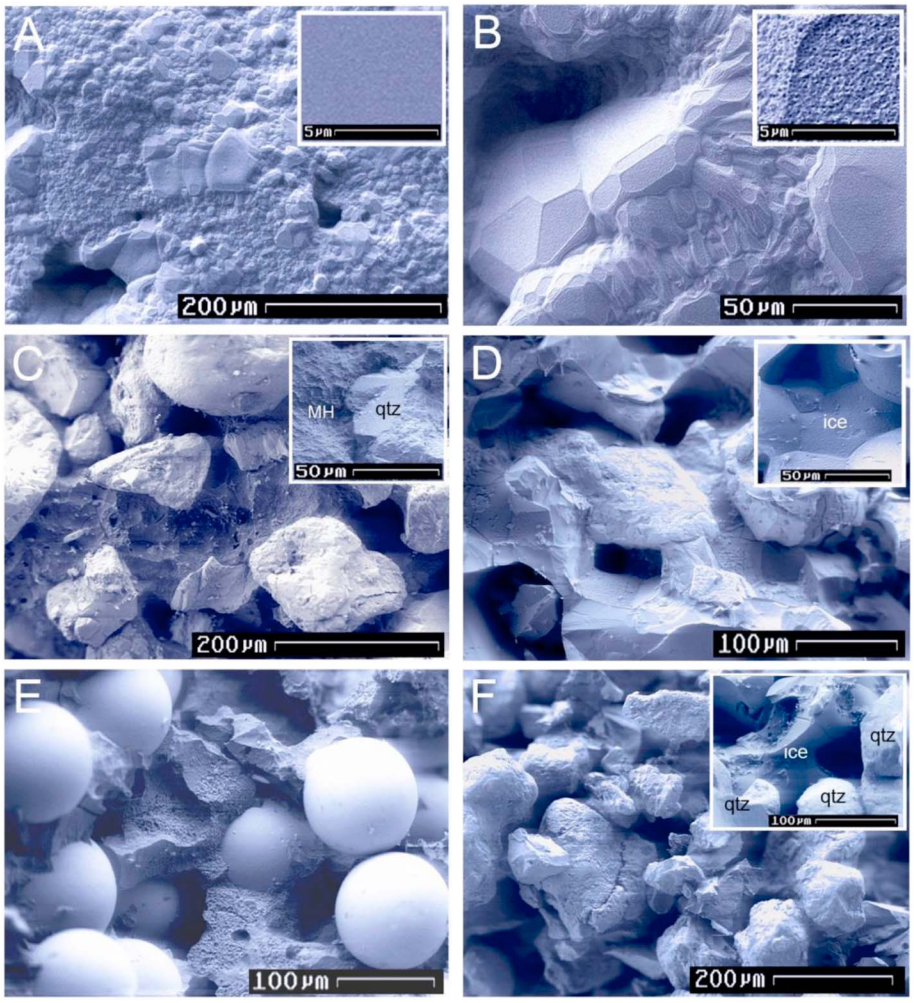

Figure 2. Cryo-SEM images of CH_4 hydrate and hydrate-sediment mixtures. (a and b) Single-phase polycrystalline CH_4 hydrate has ~20% porosity, grain size diameters of 10–80 μm, and fully dense crystals as-grown (Figure 2a, inset) that develop surface pitting with time in the high-vacuum SEM column, resulting in a nanoporous or mesoporous surface texture (Figure 2b, inset). (c) Approximately 55:45 vol % hydrate:sand (run 4) and (d) ~55:45 vol % ice:sand (run 8). Significant annealing of the ice grains accompanies dissociation at our test conditions (compare insets in Figures 2c and 2d), but there is no significant migration of sand. (e) Approximately 55:45 vol % hydrate:beads sample (run 9). SEM shows uniform distribution of components in mixed-phase samples (Figures 2c–2e) as well as similarities in the nature of the grain contacts, establishing a basis for comparison of conductivity measurements. The pitting and more porous appearance of Figure 2e is a result of sublimation of gas hydrate under high-vacuum conditions in the FE-SEM column, which is accentuated in samples with higher sediment content due to higher surface-to-volume ratio of the hydrate phase [*Stern et al.*, 2004]. (f) Approximately 10:90 vol % ice:sand (run 10) with connecting ice expanded in the inset. In Figures 2d and 2f, the samples are more porous than Figures 2a–2c because the hydrate-to-ice dissociation reaction results in a 16% volumetric reduction of the H_2O phase, as discussed in text.

also monitored sample conductivity after each incremental heating step to ensure that samples had reequilibrated to each new temperature before performing broadband measurements used to calculate electrical conductivity.

Samples containing either CH_4 hydrate or ice were recovered for cryogenic scanning electron microscope (cryo-SEM) analysis. To recover samples with CH_4 hydrate, the vessel was cooled sufficiently with liquid nitrogen (LN) prior to depressurization. CH_4 hydrate samples were then stored and transported in LN to a cryo-preparation station and imaging stage (Gatan Alto Model 2100) that in turn attached directly to a LEO982 field emission SEM. Samples were cleaved under vacuum in the preparation station to produce fresh surfaces uncontaminated by water condensation and then transferred under vacuum into the SEM

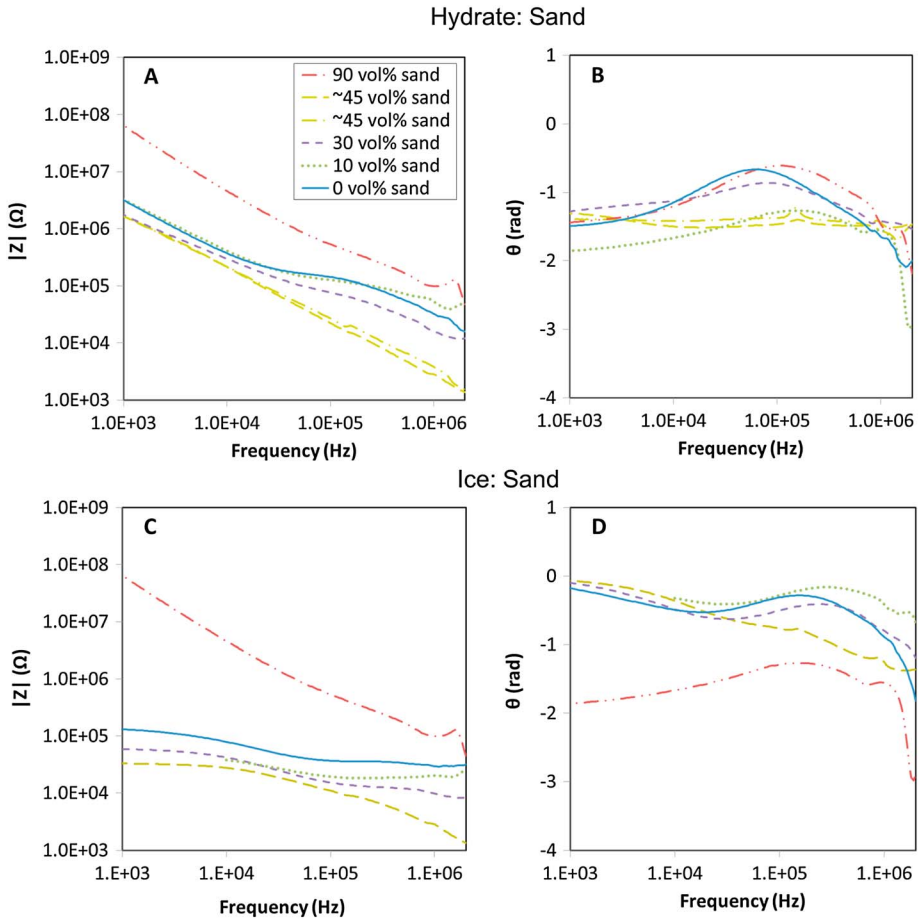

Figure 3. Total impedance magnitude ($|Z|$) and phase (θ) data as a function of frequency collected for (a and b) CH_4 hydrate: sand mixtures and (c and d) ice: sand mixtures after dissociation of CH_4. Data are plotted for CH_4 hydrate/ice without sediment as a solid blue line [*Du Frane et al.*, 2011].

column. A thermocouple embedded in the SEM sample stage recorded temperature throughout the imaging process. Imaging was conducted at temperature <-185°C, vacuum $<10^{-6}$ kPa, and accelerating voltage ≤ 2 kV. Further details of cryo-SEM imaging techniques and instrumentation are given in *Stern et al.* [2004]. Sample material was destroyed in the process of SEM imaging due to the high-vacuum environment.

3. Results

3.1. Cryogenic Scanning Electron Microscopy

Cryo-SEM images verified that the synthesized gas hydrate was fully reacted polycrystalline CH_4 hydrate (Figure 2). Sample porosity is greatly reduced in the final material due to the volumetric increase accompanying the ice to gas hydrate reaction, resulting in primarily isolated macropores (Figure 2a). Images verified that grain-scale characteristics were, in general, reproducible across all samples, with individual grains ranging from 10 to 80 μm in diameter. CH_4 hydrate grains were fully dense as grown (Figure 2a and inset), but surface pitting developed within several minutes of imaging in the high-vacuum column (Figure 2b and inset). OK#1 and glass bead sediments were uniformly distributed in mixed samples (Figures 2c–2f), thereby establishing a basis for comparison of σ measurements between mixed-phase runs. Despite annealing of ice grains accompanying dissociation, SEM images also indicated no significant migration of sediments during any given run, thus enabling comparison of σ measurements before, during, and after dissociation within a single run. The hydrate or ice grains appear to be well connected in all samples except for the one with 10:90 vol % ice:sand (Figure 2f). We were unable to evaluate subtle textural changes due to the effects of sublimation during cryo-SEM analyses. It has been

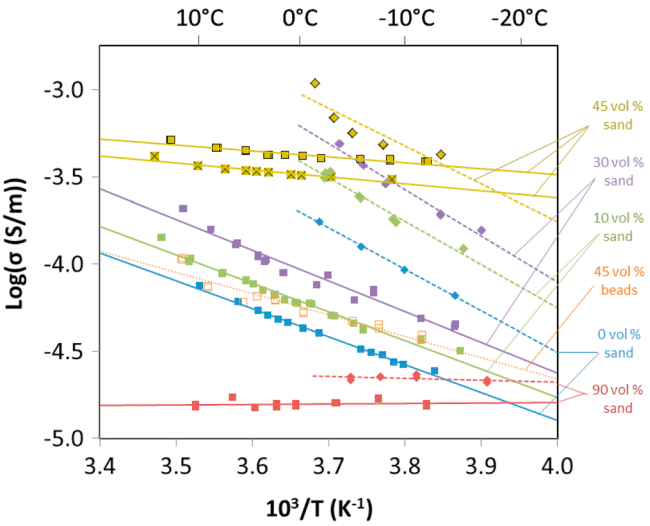

Figure 4. Electrical conductivity measurements versus inverse temperature for CH_4 hydrate in mixtures with sand (closed squares, with fits shown as solid lines) or glass beads (open squares, with fit shown as a dotted line), and ice dissociated from hydrate in mixtures with sand (filled diamonds, with fits shown as dashed lines). Two runs were performed with ~45 vol % sand: run 4 is shown as yellow squares with "Xs"; run 8 is shown as outlined, yellow squares/diamonds. Linear data fits to equation (1) are given in Table 1 with slopes that are proportional to activation energy (E_a) and intercepts equal to Log(σ_0).

previously established that our formation techniques result in samples with consistent texture, having undergone multiple cycles through the ice point with lengthy holds at the peak temperatures well above 0°C that allows samples to anneal [*Stern et al.*, 2004]. The texture of the methane hydrate in samples mixed with sand also resembles textures observed in at least some hydrate-bearing sands retrieved from nature, such as from the Alaska North Slope [*Stern et al.*, 2011].

3.2. Electrical Conductivity

The H_2O was verified to be fully reacted to CH_4 hydrate within several temperature cycles, consistent with previous studies [e.g., *Stern et al.*, 1996, 2004]. Impedance spectra were then collected on samples while heating incrementally from −15 to 15°C, with samples undergoing 7–16 temperature cycles total during the full run (Table 1). At each temperature increment, samples typically required ~1 h to reequilibrate before electrical conductivity could be measured due to the low thermal conductivity/ diffusivity of the samples [e.g., *Waite et al.*, 2007].

The addition of sediment complicated the interpretation of impedance spectra of the CH_4 hydrate. Equivalent circuit modeling of these spectra was not feasible due to the noisiness of impedance magnitude data measured at frequencies >500 kHz and <1 kHz (Figure 3a). Equivalent circuit modeling by *Du Frane et al.* [2011] for sediment-free samples indicated that the impedance magnitude associated with the maximum phase angle could be used to avoid systemic effects due to the electrodes and their leads (see Figure 3a in *Du Frane et al.* [2011]). For CH_4 hydrate mixed with sediments, the phase angle data show maxima at intermediate frequencies on the order of ~100 kHz similar to pure CH_4 hydrate samples (Figure 3b). This was also the case after dissociation of CH_4 hydrate to ice (Figures 3c and 3d). Based on these observations, we similarly used phase angle to determine the correct frequency to calculate electrical conductivity.

Electrical conductivity of mixtures generally exhibited exponential dependence on temperature both after CH_4 hydrate formation, and after dissociation to ice, which is typical for electrolytic materials. We fit data using an Arrhenius expression,

$$\sigma(T) = \sigma_0 e^{-E_a/RT} \quad (1)$$

where σ_0 is a preexponential constant (S/m), E_a is the activation energy (kJ/mol), R is the gas constant (8.314 J/mol/K), and T is the temperature (K). Plotting Log(σ) versus $10^3/T$(K) gives slopes that are proportional to E_a (Figure 4). Table 1 gives fitted parameters for σ_0 and E_a for each sample mixture that can be used to calculate electrical conductivity as function of temperature.

Increased sand concentrations of up to ~45 vol % in mixtures with CH_4 hydrate resulted in increased conductivity of the overall mixtures (runs 4, 5, 6, and 8; Table 1 and Figure 4). Conversely, the sample with 10:90 vol % CH_4 hydrate:sand (run 10) had much lower conductivity. SEM images indicate that dissociated ice, and likely CH_4 hydrate, was poorly connected in this sample (Figure 2f), in which case surface conductivity through the well-connected sand may have a nonnegligible contribution to the electrical conductivity of the mixture [e.g., *Wildenschild et al.*, 2000; *Revil et al.*, 2014]. Activation energy decreased substantially with increasing sand, from 30.6 kJ/mol for pure CH_4 hydrate to 7.66 kJ/mol for a

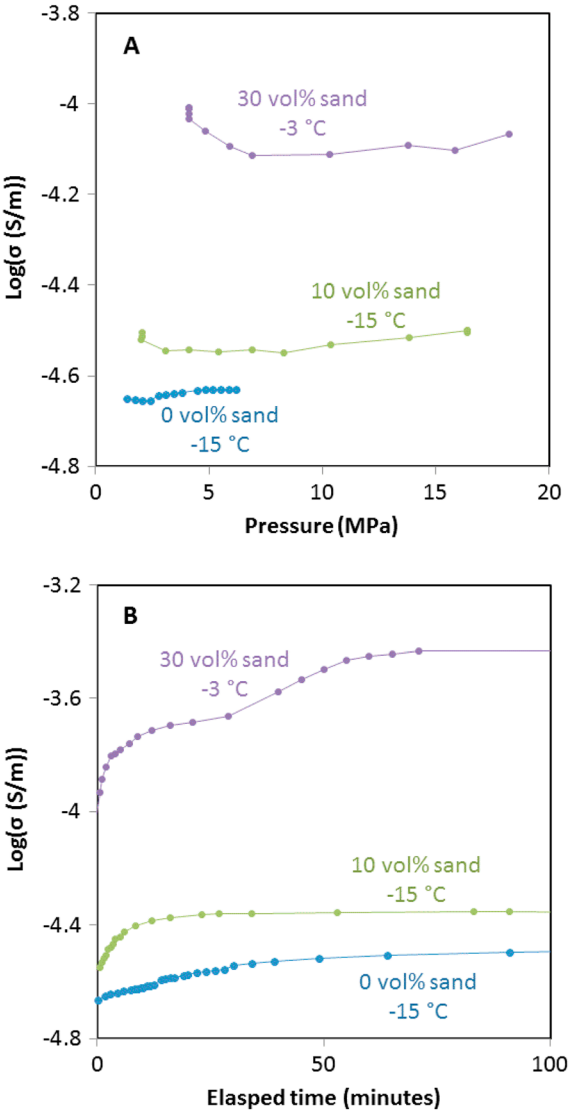

Figure 5. Electrical conductivity of sample mixtures during dissociation of CH_4 hydrate back into ice as (a) a function of pressure and as (b) a function of elapsed time. Samples dissociated at a significantly higher rate at −3°C than at −15°C.

sample containing ~45 vol % sand. The CH_4 hydrate + sand mixtures showed little σ change as we vented CH_4 to approach the edge of the stability field (Figure 5a), indicating that the effects of pressure are small in the range of these experiments. Once the CH_4 gas was fully vented, electrical conductivity slowly began to increase as the CH_4 hydrate in samples dissociated to ice (Figure 5b). The presence of sand produced similar σ increases after dissociation of CH_4 hydrate to ice but had less effect on E_a.

Two experiments (runs 7 and 9) were conducted using ~45 vol % glass beads of similar grain size as OK#1 for comparison to runs with sand. Run 9 showed that glass beads had less overall effect on electrical properties of CH_4 hydrate than sand (Figure 4); mixing glass beads into CH_4 hydrate led to only a slight increase in overall electrical conductivity and a slight decrease in activation energy. The glass beads are less angular and consequently will have less connectivity than sand for a given volume percentage. However, SEM images (Figures 2c and 2e) indicate that both sand and glass beads are well connected at ~45 vol %. Small differences in connectivity past the percolation threshold are unlikely to account for the substantially larger effects that sand has on electrical conductivity of mixtures with CH_4 hydrate relative to glass beads (Figure 4), but further studies are needed to fully evaluate the effects of angularity and grain orientation. Ion chromatography (IC) and total inorganic carbon analyses conducted on select samples that were dissociated after testing (runs 3, 5, 6, and 7) verified that significant amounts of ionic impurities were present on the surfaces of both the sand and glass beads (data presented in supporting information). These data were used also to calculate pH using the EQ3/6 software package [*Wolery*, 1992] (see supporting information).

4. Discussion

Electrical conductivity measurements on water-free CH_4 hydrate + sediment mixtures in this study are predictably lower in magnitude than those previously reported for water-bearing mixtures [*Spangenberg and Kulenkampff*, 2006; *Ren et al.*, 2010; *Li et al.*, 2012]. The σ of CH_4 hydrate with ~45 vol % quartz sand (OK#1) is 1 order of magnitude lower than a measurement of $10^{-2.42}$ S/m reported for 62 vol % glass beads packs saturated with 36 vol % CH_4 hydrate and 2 vol % water [*Spangenberg and Kulenkampff*, 2006]. Measurements on sand packs saturated with ~10 vol % CH_4 hydrate and ~20 vol % water are on the order of $10^{-0.5}$ S/m at 5°C [*Ren et al.*, 2010], significantly higher than measurements on water-free mixtures.

Unexpectedly, the addition of sediment in the form of quartz sand and glass beads increased the overall electrical conductivity of most sample mixtures with CH_4 hydrate or ice (Figure 4). This is somewhat

counterintuitive because quartz sand and silica beads by themselves have low electrical conductivity. The one exception was the mixture with 90 vol % sand that had significantly lower electrical conductivity than other sample mixtures. Ice appeared poorly connected within this mixture in SEM images (Figure 2f), suggesting that this high concentration of sand exceeds the percolation threshold (i.e., the concentration required for connectivity) for both the dissociated ice and CH_4 hydrate. This indicates that the CH_4 hydrate or ice grains provided the primary path for current when connected through sample mixtures, although the presence of sediment raised total electrical conductivity. The increase to electrical conductivity by the presence of ~45 vol % glass beads was significant (run 9), but substantially lower than the effects of naturally weathered quartz sand (Figure 4).

Electrical conductivity was likely enhanced in the CH_4 hydrate grains by impurities that were introduced from weathered surfaces of the sand. Ionic doping of the CH_4 hydrate grains could explain why activation energies decreased with increased sand concentrations. The activation energy contains two physical phenomena: an increase in defect mobility with temperature and an increase in defect population with temperature. These impurities are likely to have low mobility but are charge-compensated by protonic defects that have relatively high mobility. When there are few to no impurities present, protonic defects are likely to be thermally induced in the gas hydrate structure, which would make electrical conductivity strongly dependent on temperature. If the structure is doped with impurities there could be a population of protonic defects induced to maintain charge balance that are relatively insensitive to temperature. Doping would cause electrical conductivity to increase substantially with a population of charge carriers that mask those that are thermally induced, yielding electrical conductivity with less temperature dependence, i.e., lower activation energy. The electrical conductivity of CH_4 hydrate + sand mixtures was substantially higher than pure CH_4 hydrate (Figure 4), which indicates that some impurities from sand can be included in CH_4 hydrate. Probable candidates include ions that were found in higher concentrations on the surfaces of the sand compared with those on the surface of glass beads: K^+, Ca^{2+}, Mg^{2+}, NH_4^+, Cl^-, and SO_4^{2-} (Table S1 in the supporting information). Most impurities that are dissolved in water become excluded during ice crystallization, with the exception of a few acids (HF and HCl), ammonia (NH_3), alkalis (KOH and NaOH), and their derivatives (NH_4F or KCl) that drastically change the protonic carrier concentration [e.g., *Petrenko and Whitworth*, 1999]. KOH inclusion into THF hydrate has also been demonstrated to trigger formation of charge carriers, Bjerrum and protonic defects, and could also affect mobilities of other point defects [*Nelson et al.*, 2013]. If CH_4 hydrate behaves similar to ice, then the sand may have contributed KOH and its derivative KCl during synthesis, which is consistent with IC detection of both K^+ water melted from samples containing sand (runs 5 and 6), but not in those containing glass beads (run 7) or in those that did contain any sediment (run 3) (Table S1). It would also be expected that NaCl and Na_2CO_3 would be excluded during its crystallization. Inclusion of K^+ and Cl^- is thus one possible explanation for what caused the observed doping effect on the electrical conductivity of CH_4 hydrate-sand mixtures.

A first-order model of the doping effect on the electrical conductivity of CH_4 hydrate and ice caused by impurities from sand is presented in section S2 in the supporting information. The model includes a second conductivity term that is proportional to sand concentration and assumes a simple parallel mixing law relationship. We were able to obtain excellent fits to data for sample mixtures with 10 or 30 vol % sand but not for those with ~45 or 90 vol % sand. This is because mixing laws are typically incapable of expressing behavior across percolation thresholds. If impurities do not move far from the sand surface, CH_4 hydrate/sand interfaces may have higher electrical conductivity than the bulk conductivity of CH_4 hydrate grains. If both CH_4 hydrate and sand are interconnected, then interfaces between the two phases will also be interconnected possibly creating a high conductivity path throughout mixtures. This could explain the large increase in electrical conductivity and decrease in activation energy when increasing the amount of sand in mixtures from 30 to ~45 vol %. Therefore, the model is only applicable to scenarios where hydrate/ice is well connected in mixtures, but the sediment is not, and should be considered preliminary at best given the limited range of compositions examined here.

The results of this study imply that sediment composition, in addition to sediment amount and distribution, will be a critical factor in determining bulk electrical conductivity of gas hydrates, at least in sections devoid of pore water. In nature, impurities could be acquired from sediments, organic material, or pore water itself. While gas hydrate formation is typically viewed as a purification process—a promising aspect that can

potentially be exploited for desalination of highly saline wastewater into potable water [*Cha and Seol*, 2013]—our results suggest that even trace amounts of impurities incorporated within the CH_4 hydrate lattice produce substantial effects on the overall electrical properties of CH_4 hydrate. The OK#1 and glass beads were chosen for this study because they are regarded to have high purity in comparison to most sediment and facilitated our attempt to study the fundamental contributions of individual conduction mechanisms to total conductivity. In contrast, sediments found in permafrost and marine settings have the potential to contribute different and larger concentrations of impurities. Pore water may also contribute impurities in amounts substantial enough to affect the electrical properties, although this effect would likely be masked in comparison with the effect of the pore water itself. For example, seawater contains roughly 400 mg/L of K^+ [*Webb*, 1939], which is within the range of measured values for water melted from the postrun samples (Table S1). Physical and chemical conditions will also play a role in what concentrations of impurities are included during gas hydrate formation. Chemical transfer of ionic impurities must be carefully considered to accurately determine the electrical conductivity of gas hydrate formations in marine sediments.

5. Conclusions

The electrical conductivity of liquid-free CH_4 hydrate-sediment mixtures is highly dependent on composition and temperature. Increasing sand concentrations up to 45 vol % increased the overall electrical conductivity of mixtures by as much as an order of magnitude at 0°C. The overall electrical conductivity of mixtures plummeted in a sample containing a sufficiently high sediment concentration (90 vol %) that crossed a percolation threshold, such that the CH_4 hydrate was poorly connected. This observation provides evidence that CH_4 hydrate (and ice after dissociation) is the primary current path within mixtures.

Ionic impurities from sand caused a doping effect on the electrical properties of CH_4 hydrate (and ice). This is consistent with the observation that increasing sand content in mixtures resulted in higher-magnitude electrical conductivity and less temperature dependence, i.e., lower activation energy values. Over the range of geologically relevant temperatures from −5 to 15°C, the overall electrical conductivity of CH_4 hydrate mixtures with ≤30 vol % sand increased by ~3 times. Mixtures with ≥45 vol % CH_4 hydrate exhibited almost no change in conductivity over that same range. Most of the ionic impurities associated with the glass beads appear to have been excluded during CH_4 hydrate formation (Na^+, CO_3^{2-}, and HCO_3^-), while at least some of the ionic impurities more strongly associated with the sand grains were included (K^+, Ca^{2+}, Mg^{2+}, NH_4^+, Cl^-, and SO_4^{2-}).

The addition of sediments to samples is the methodical second step in the evolution of this work, following our initial measurements of pure, end-member CH_4 hydrate. While these results can only be loosely applied to "dry" systems with essentially no pore water present, they are necessary experiments to increase the fundamental understanding of individual conduction mechanisms and the properties of mixtures in these systems. Future tests involving the controlled addition of liquid water with varying salinities will be necessary for further application to complex natural systems.

Acknowledgments
The authors thank S. Roberts (LLNL) for assisting with ion chromatography measurements; W. Durham (MIT) for providing the OK#1 sand used in this study; J. Pinkston, S. Kirby, D. Lockner, W. Waite, and A. Hunt (U. S. Geological Survey) for their helpful discussions, advice, and reviews; and J. Lemire (Scripps Institution of Oceanography) for the help with the cell fabrication and design. Data supporting Figures 3–5 are available in the supporting information. Support for this work was provided by DOE contract DE-NT0005668 awarded to S. Constable (SIO) and Interagency Agreement DE-NT0006147 between the USGS Gas Hydrate Project and the DOE's Methane Hydrate R&D Program. Prepared by LLNL under contract DE-AC52-07NA27344. The use of trade, product, industry, or firm names in this report is for descriptive purposes only and does not constitute endorsement by the U.S. Geological Survey or the U.S. Government.

References

Archie, G. E. (1942), The electrical resistivity log as an aid in determining some reservoir characteristics, *Trans. Am. Inst. Min. Metall. Pet. Eng.*, *146*, 54–62.

Boswell, R., and T. Collett (2011), Current perspectives on gas hydrate resources, *Energy Environ. Sci.*, *4*, 1206–1215.

Cha, J.-H., and Y. Seol (2013), Increasing gas hydrate formation temperature for desalination of high salinity produced water with secondary guests, *ACS Sustainable Chem. Eng.*, *1*(10), 1218–1224.

Collett, T. (2002), Energy resource potential of natural gas hydrate, *Am. Assoc. Pet. Geol. Bull.*, *86*, 1971–1992.

Collett, T. S., and J. W. Ladd (2000), Detection of gas hydrate with downhole logs and assessment of gas hydrate concentrations (saturations) and gas volumes on the Blake Ridge with electrical resistivity log data, *Proc. Ocean Drill. Program Sci. Results*, *164*, 179–191.

Du Frane W. L., L. A. Stern, K. A. Weitemeyer, S. Constable, J. C. Pinkston, and J. J. Roberts (2011), Electrical properties of polycrystalline methane hydrate, *Geophys. Res. Lett.*, *38*, L09313, doi:10.1029/2011GL047243.

Durham, W. B., A. V. Pathare, L. A. Stern, and H. J. Lenferink (2009), Mobility of icy sand packs, with application to Martian permafrost, *Geophys. Res. Lett.*, *36*, L23203, doi:10.1029/2009GL040392.

Dvorkin, J., M. B. Helgerud, W. F. Waite, S. H. Kirby, and A. Nur (2000), Introduction to physical properties and elasticity models, in *Natural Gas Hydrate In Oceanic and Permafrost Environments*, edited by M. D. Max, pp. 245–260, Kluwer Acad., Dordrecht, Netherlands.

Edwards, R. N. (1997), On the resource evaluation of marine gas hydrate deposits using sea-floor transient electric dipole-dipole methods, *Geophysics*, *62*(1), 63–74.

Ellis, M. H., T. A. Minshull, M. C. Sinha, and A. I. Best (2008), Joint seismic/electrical effective medium modelling of hydrate-bearing marine sediments and an application to the Vancouver Island margin, in *Proceedings of the 6th International Conference on Gas Hydrates*, 5586–[12p], Vancouver, Canada.

Evans, R. L. (2007), Using CSEM techniques to map the shallow section of seafloor: From the coastline to the edges of the continental slope, *Geophysics*, *72*(2), WA105–WA116.

Glover, P. W. J., M. J. Hole, and J. Pous (2000), A modified Archie's law for two conducting phases, *Earth Planet. Sci. Lett.*, *180*, 369–383.

Hashin, Z., and S. Shtrikman (1962), A variational approach to the theory of effective magnetic permeability of multiphase materials, *J. Appl. Phys.*, *33*, 3125–3131.

Hornbach, M. J., W. S. Holbrook, A. R. Gorman, K. L. Hackwith, D. Lizarralde, and I. Pecher (2003), Direct seismic detection of methane hydrate on the Blake Ridge, *Geophysics*, *68*(1), 92–100.

Kneafsey, T. J., Y. Seol, A. Gupta, and L. Tomutsa (2011), Permeability of laboratory-formed methane-hydrate-bearing sand: measurements and observations using X-ray computed tomography, *SPE J.*, *16*(1), 78–94.

Kvenvolden, K., and T. Lorenson (2001), The global occurrence of natural gas hydrate, in *Natural Gas Hydrates: Occurrence, Distribution, and Detection*, *Geophys. Monogr. Ser.*, vol. 124, edited by C. Paull and W. Dillon, pp. 87–98.

Kvenvolden, K. A. (1999), Potential effects of gas hydrate on human welfare, *Proc. Natl. Acad. Sci. U.S.A.*, *96*(7), 3420–3426.

Lee, J. Y., J. C. Santamarina, and C. Ruppel (2010), Parametric study of the physical properties of hydrate-bearing sand, silt, and clay sediments: 1. Electromagnetic properties, *J. Geophys. Res.*, *115*, B11104, doi:10.1029/2009JB006669.

Li, F. G., C. Y. Sun, S. L. Li, G. J. Chen, X. Q. Guo, L. Y. Yang, H. Pan, S. Li, and K. Zhang (2012), Experimental studies on the evolvement of electrical resistivity during methane hydrate formation in sediments, *Energy Fuels*, *26*, 6210–6217.

Maslin, M., M. Owen, R. Betts, S. Day, T. Dunkley Jones, and A. Ridgwell (2010), Gas hydrates: Past and future geohazard?, *Proc. R. Soc. A*, *368*(1919), 2369–2393.

Milkov, A. V. (2004), Global estimates of hydrate-bound gas in marine sediments: How much is really out there?, *Earth Sci. Rev.*, *66*(3–4), 183–197.

Nelson, H., S. Schildmann, A. Nowaczyk, C. Gainaru, B. Geil, and R. Bohmer (2013), Small-angle water reorientations in KOH doped hexagonal ice and clathrate hydrates, *Phys. Chem. Chem. Phys.*, *15*, 6355–6367.

NIIR Board of Consultants & Engineers (2005), *The Complete Book on Glass and Ceramics Technology*, 624 pp., Asia Pacific Business Press, New Dehli.

Petrenko, V. F., and R. W. Whitworth (1999), *Physics of Ice*, Oxford Univ. Press, New York.

Ren, S. R., Y. Liu, and W. Zhang (2010), Acoustic velocity and electrical resistance of hydrate bearing sediments, *J. Petrol. Sci. Eng.*, *70*, 52–56.

Revil, A., P. Kessouri, and C. Torres-Verdín (2014), Electrical conductivity, induced polarization, and permeability of the Fontainebleau sandstone, *Geophysics*, *79*(5), D301–D318.

Roberts, J. J. (2002), Electrical properties of microporous rock as a function of saturation and electrical conductivity, *J. Appl. Phys.*, *91*(3), 1687–1694.

Roberts, J. J., and J. A. Tyburczy (1991), Frequency-dependent electrical-properties of polycrystalline olivine compacts, *J. Geophys. Res.*, *96*(B10), 16,205–16,222, doi:10.1029/91JB01574.

Roberts, J. J., and J. A. Tyburczy (1993), Impedance spectroscopy of single and polycrystalline olivine: Evidence for grain-boundary transport, *Phys. Chem. Miner.*, *20*(1), 19–26.

Ruppel, C. (2007), Tapping methane hydrates for unconventional natural gas, *Elements*, *3*(3), 193–199.

Schwalenberg, K., E. Willoughby, R. Mir, and R. N. Edwards (2005), Marine gas hydrate electromagnetic signatures in Cascadia and their correlation with seismic blank zones, *First Break*, *23*, 57–63.

Sloan, E., and C. Koh (2007), *Clathrate Hydrates of Natural Gases*, 3rd ed., p. 721, Taylor and Francis, CRC Press, Boca Raton, Fla.

Spangenberg, E., and J. Kulenkampff (2006), Influence of methane hydrate content on electrical sediment properties, *Geophys. Res. Lett.*, *33*, L24315, doi:10.1029/2006GL028188.

Stern, L. A., S. H. Kirby, and W. B. Durham (1996), Peculiarities of methane clathrate hydrate formation and solid-state deformation, including possible superheating of water ice, *Science*, *273*(5283), 1843–1848.

Stern, L. A., S. H. Kirby, S. Circone, and W. B. Durham (2004), Scanning electron microscopy investigations of laboratory-grown gas clathrate hydrates formed from melting ice, and comparison to natural hydrates, *Am. Mineral.*, *89*(8–9), 1162–1175.

Stern, L. A., T. D. Lorenson, and J. C. Pinkston (2011), Gas hydrate characterization and grain-scale imaging of recovered cores from the Mount Elbert Gas Hydrate Stratigraphic Test Well, Alaska North Slope, *Mar. Pet. Geol.*, *28*, 394–403.

Waite, W. F., L. A. Stern, S. H. Kirby, W. J. Winters, and D. H. Mason (2007), Simultaneous determination of thermal conductivity, thermal diffusivity and specific heat in sI methane hydrate, *Geophys. J. Int.*, *169*(2), 767–774.

Wallmann, K., E. Pinero, E. Burwicz, M. Haeckel, C. Hensen, A. Dale, and L. Ruepke (2012), The global inventory of methane hydrate in marine sediments: A theoretical approach, *Energies*, *5*, 2449–2498.

Webb, D. A. (1939), The sodium and potassium content of sea water, *J. Exp. Biol.*, *16*, 178–183.

Weitemeyer, K. A., S. C. Constable, K. W. Key, and J. P. Behrens (2006), First results from a marine controlled-source electromagnetic survey to detect gas hydrates offshore Oregon, *Geophys. Res. Lett.*, *33*, L03304, doi:10.1029/2005GL024896.

Weitemeyer, K. A., S. Constable, and A. M. Tréhu (2011), A marine electromagnetic survey to detect gas hydrate at Hydrate Ridge, Oregon, *Geophys. J. Int.*, doi:10.1111/j.1365-246X.2011.05105.x.

Wildenschild, D., J. J. Roberts, and E. D. Carlberg (2000), On the relationship between microstructure and electrical and hydraulic properties of sand-clay mixtures, *Geophys. Res. Lett.*, *27*(19), 3085–3088, doi:10.1029/2000GL011553.

Wolery, T. W. (1992), EQ3/6, a software package for geochemical modeling of aqueous systems; UCRL MA-110662-PT-1; Lawrence Livermore National Laboratory, Livermore, Calif.

Zhang, Z. J., and G. A. McMechan (2006), Elastic inversion for distribution of gas hydrate, with emphasis on structural controls, *J. Seismic Explor.*, *14*(4), 349–370.